Model Calculations of Magnetic Band Structure*

FRANK A. BUTLER† AND E. BROWN
Rensselaer Polytechnic Institute, Troy, New York
(Received 5 July 1967)

Simple model effective Hamiltonians are used to examine the structure of magnetic sub-bands. The positions of the discrete Landau levels are shown to be accurately predicted by the first-order correction to the Onsager quantization rule given by Roth, even for strong magnetic fields. The influence of the rational field condition, occuring when l/N flux quanta pass through a unit cell, is investigated. The effect is pronounced when intraband or interband tunneling occurs. In this case the broadened sub-bands split into a cluster of l smaller sub-bands. This fine structure may be roughly accounted for by use of an effective Hamiltonian based on the sub-band energy function $E(\mathbf{q})$.

I. INTRODUCTION

THE electronic energy spectra of crystals in magnetic fields can be conveniently studied by means of an effective Hamiltonian, in which the spectrum is obtained as eigenvalues of an operator $H(\boldsymbol{\pi})$. Here $\boldsymbol{\pi}$ is the operator $\mathbf{p}+e\mathbf{A}/c$, where e is the magnitude of the electronic charge and $\mathbf{A}$ is the vector potential. As shown previously,[1] this formulation is valid for arbitrary magnetic fields.[2] In principle, the operator H is a matrix function of $\boldsymbol{\pi}$ whose elements depend explicitly on the magnetic field. When written in diagonal form, however, it is usually sufficient to approximate the diagonal elements by the single-band effective Hamiltonian $E^n(\boldsymbol{\pi})$ obtained by replacing $\mathbf{k}$ by the operator $\boldsymbol{\pi}$ in the energy-band function $E^n(\mathbf{k})$ of the nth band. This approximation is good for structure associated with isolated bands. In this paper a one-band model effective Hamiltonian is used to investigate certain features of this structure. For states near the bottom or the top of the band one expects a free-electron model, with the appropriate effective mass, to provide a fairly accurate description. The spectrum associated with motion perpendicular to the magnetic field is expected to be characterized by evenly spaced discrete Landau levels, whose spacing is proportional to the field strength. This is consistent with Onsager's area quantization condition.[3] A more rigorous analysis by Roth[4] showed that one should expect Onsager's rules to be only a zeroth-order approximation to the true spectrum, in general. She has given a correction formula which is a power series in the magnetic field. Accurate calculations on a simple model afford a test of the accuracy of these correction terms.

Another problem which is treated here arises in connection with the structure of broadened magnetic sub-bands. These are associated with a region of an energy band in which the energy contours in momentum space form open orbits, or nearly touching orbits, in a repeated zone scheme. The structure of these broadened sub-bands are expected to be quite sensitive to the ratio l/N, discussed in an accompanying paper[5] for rational fields. The splitting of the sub-bands into smaller ones has been discussed by several authors.[6,7] In particular Azbel[8] has examined this one point analytically. Model calculations based on the effective Hamiltonian are particularly simple in the case of rational fields, since in that case, the difference equation one gets from the effective Hamiltonian is equivalent to obtaining eigenvalues of a finite matrix, and can be done by routine methods.

Calculations were carried out also on a two-band model to examine the onset of breakdown associated with interband as well as intraband tunneling.

II. ONE- AND TWO-BAND EFFECTIVE HAMILTONIANS

The one-band effective Hamiltonian can be written as

$$H(\boldsymbol{\pi})=\sum_{\mathbf{R}} \epsilon(\mathbf{R})e^{i\mathbf{R}\cdot\boldsymbol{\pi}}, \tag{1}$$

where we have chosen units with $\hbar=1$. The coefficients $\epsilon(\mathbf{R})$ are field-dependent in general, but can be assumed to be closely approximated by the Fourier coefficients of $E(\mathbf{k})$. We thus make the assumption

$$E(\mathbf{k})=\sum_{\mathbf{R}} \epsilon(\mathbf{R})e^{i\mathbf{R}\cdot\mathbf{k}}. \tag{2}$$

We can also take a different point of view. We know that there exists a set of coefficients $\epsilon(\mathbf{R})$ which leads to a valid effective Hamiltonian for a given magnetic field. The function $E(\mathbf{k})$ defined by Eq. 2 would not necessarily be the correct energy-band function appropriate to zero fields, but it would probably be the one deduced from experiments done at this field value, or close to it. In our calculations the Fourier coefficients $\epsilon(\mathbf{R})$ are taken as parameters of the model.

* Supported by the U. S. Atomic Energy Commission.
† Present address: University of Kentucky, Lexington, Ky.
[1] E. Brown, Phys. Rev. **133**, A1038 (1964).
[2] The effective Hamiltonian has only been proven to be valid when the magnetic flux through any two-dimensional unit cell is a rational number, when expressed in flux quanta. Any real field can be approximated to arbitrary accuracy by one satisfying these conditions.
[3] L. Onsager, Phil. Mag. **43**, 1006 (1952).
[4] L. M. Roth, Phys. Rev. **145**, 434 (1966).
[5] E. Brown, preceding paper, Phys. Rev. **166**, 626 (1968).
[6] W. G. Chambers, Phys. Rev. **140**, A135 (1965).
[7] E. I. Blount, Phys. Rev. **126**, 1636 (1962).
[8] M. Ya. Azbel, Zh. Eksperim. i Teor. Fiz. **46**, 929 (1964) [English transl.: Soviet Phys.—JETP **19**, 634 (1964)].

We require the eigenvalues of

$$H(\boldsymbol{\pi})\psi(\mathbf{r})=E\psi(\mathbf{r}). \tag{3}$$

Although this has the appearance of Schrödinger's equation, the operator $H(\boldsymbol{\pi})$ only couples points separated by a lattice vector. Thus, this is, in reality, a difference equation with $\psi(\mathbf{r})$ defined only at lattice points. The components of $\boldsymbol{\pi}$ commute with each of the components of the operator $(\boldsymbol{\pi}+e\mathbf{r}\times\mathbf{B}/c)$. We can pick $\psi(\mathbf{r})$ as a simultaneous eigenfunction of two of these components, one along $\mathbf{a}_3$, the direction of $\mathbf{B}$, the other along $\mathbf{a}_1$. For rational fields, in which

$$\phi\equiv\mathbf{B}\cdot(\mathbf{a}_1\times\mathbf{a}_2)e/\hbar c=2\pi l/N, \tag{4}$$

we can impose the additional requirement[1] that $\psi(\mathbf{r})$ goes into a multiple of itself under magnetic translations through $N\mathbf{a}_2$. This follows from the invariance properties of $H(\boldsymbol{\pi})$ under magnetic translations. We can then characterize the solutions by a wave vector $\mathbf{q}$. Making use of these facts Eq. (3) can be transformed into

$$\sum_{m,n_1,n_3}\epsilon[n_1\mathbf{a}_1+(m-n)\mathbf{a}_2+n_3a_3]\times\exp\{-i[n_1\mathbf{q}_1\cdot\mathbf{a}_1+n_3\mathbf{q}_3\cdot\mathbf{a}_3+\tfrac{1}{2}n_1(n+m)\phi]\}U_m=EU_n, \tag{5}$$

with the boundary condition

$$U_{n+N}=e^{iN\mathbf{q}_2\cdot\mathbf{a}_2}U_n. \tag{6}$$

As previously shown, the domain of $\mathbf{q}$ is a magnetic zone, which is smaller than a Brillouin zone by a factor N in each of the directions normal to the field. Equations (5) and (6) are equivalent to an N-dimensional matrix equation. We can carry out the sum over n_3 immediately obtaining

$$\sum_{m,n_1}\epsilon_{\mathbf{q}_3}[n_1\mathbf{a}_1+(m-n)\mathbf{a}_2]\times\exp\{-i[n_1\mathbf{q}_1\cdot\mathbf{a}_1+\tfrac{1}{2}n_1(n+m)\phi]\}U_m=EU_n. \tag{7}$$

Since we are going to parametrize the Fourier coefficients anyway we disregard the dependence on $\mathbf{q}_3$ and write

$$\epsilon_{\mathbf{q}_3}(n_1\mathbf{a}_1+n_2\mathbf{a}_2)\equiv\epsilon(n_1,n_2). \tag{8}$$

In our first model calculation we choose a simple cubic lattice with $\mathbf{B}$ along z, one of the cube axes. We define

$$\epsilon(\pm1,0)=\epsilon(0,\pm1)\equiv\epsilon, \tag{9}$$

with the remaining coefficients zero. The corresponding two-dimensional energy-band function is

$$E(k_x,k_y)=2\epsilon(\cos k_xa+\cos k_ya). \tag{10}$$

The eigenvalue equation is transformed into a form suitable for calculation in the Appendix. Numerical calculations were carried out for $\epsilon=-1$, with $l/N=1/50$ and $3/151$. In Fig. 1 we have shown one quadrant of the energy-band function $E(\mathbf{k})$ for this choice. The calculated energy levels are shown in Fig. 2. The results are symmetric about $E=0$. As expected the levels are discrete except in the neighborhood of the extended orbit, corresponding to zero energy in Fig. 1. The discrete levels for $l/N=1/50$ are given in the first column of Table I. In order to compare with the Onsager predictions we calculated the area enclosed by the contours in Fig. 1 whose energy corresponded to the

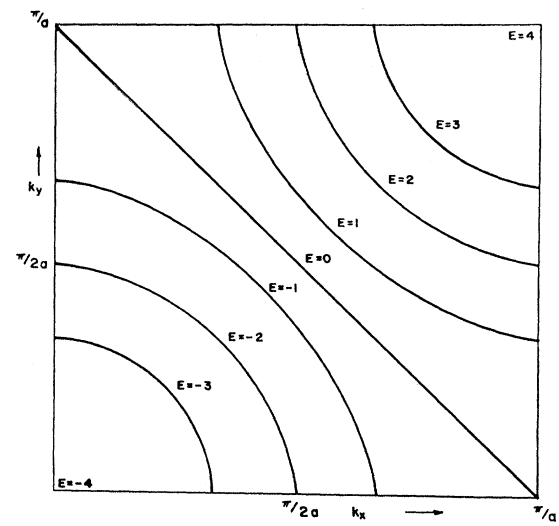

FIG. 1. Energy contours for single-band model (one-quarter of Brillouin zone).

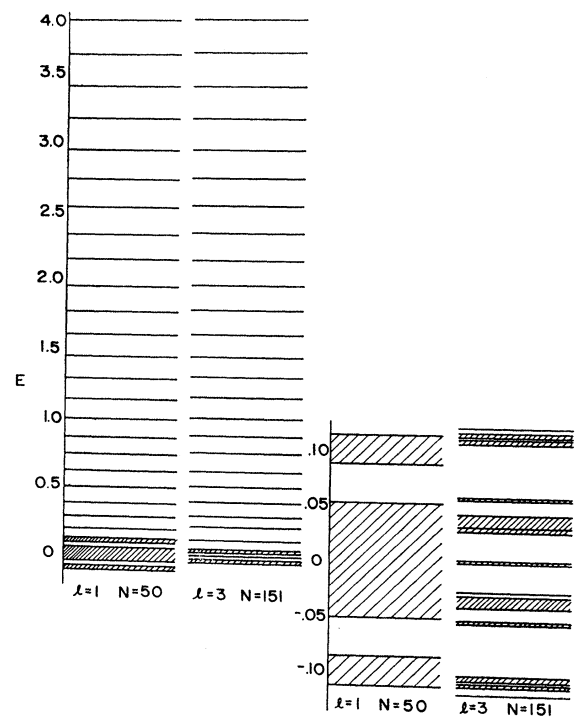

FIG. 2. Magnetic sub-bands and discrete Landau levels for single-band model. The magnetic field is given by $B=l/N(hc/ea^2)$. The structure is symmetric about $E=0$.

TABLE I. Discrete levels and corresponding orbit areas for a simple square lattice ($l/N=1/50$).

n	$-E_n$	a^2A_n	$a^2(A_n-A_n^0)$ (10^{-3})	Roth correction[a] (10^{-3})
1	3.87630	0.39166	−3.13	−3.13
2	3.63279	1.18117	−3.18	−3.18
3	3.39699	1.97068	−3.24	−3.24
4	3.16880	2.76017	−3.32	−3.32
5	2.94809	3.54966	−3.40	−3.40
6	2.73477	4.33913	−3.50	−3.50
7	2.52873	5.12859	−3.61	−3.60
8	2.32988	5.91803	−3.74	−3.73
9	2.13813	6.70744	−3.89	−3.89
10	1.95340	7.49683	−4.07	−4.07
11	1.77562	8.28619	−4.28	−4.28
12	1.60473	9.07550	−4.54	−4.54
13	1.44068	9.86475	−4.85	−4.85
14	1.28342	10.65394	−5.24	−5.23
15	1.13295	11.44303	−5.72	−5.70
16	0.98926	12.23199	−6.32	−6.30

[a] Reference 4.

calculated eigenvalues. The area of the nth contour according to Onsager[3] should be

$$A_n^0=(n-\tfrac{1}{2})(l/N)(2\pi/a)^2, \tag{11}$$

where the lowest eigenvalue corresponds to $n=1$. The discrepancy is shown in Table I along with the second-order correction given by Roth.[4] The Onsager rules are seen to be quite accurate. The Roth correction, however, brings the theoretical results into almost perfect agreement with the calculations. It should be noted that the value $l/N=1/50$ corresponds to magnetic fields several orders of magnitude larger than are presently available.

Although it is not apparent from Fig. 2, there are N magnetic sub-bands in the spectrum coming from one band. For the case $l/N=1/50$ there are two bands which touch at $E=0$. For the case $l/N=3/151$ each of the discrete levels corresponds to three magnetic sub-bands, which are almost exactly degenerate (almost no measurable spread to the accuracy of our calculations). We can think of this spectrum as arising from the former one (except for a slight shift) by having each sub-band decompose into three, with one extra band centered at $E=0$. The splitting of the broadened bands are shown on an enlarged scale in the right half of Fig. 2.

The structure $E(\mathbf{q})$ of the broadened magnetic sub-band near $E=0$ is shown in Figs. 3 and 4. The contours for each magnetic sub-band of this simple effective Hamiltonian are identical. In other words, for any sub-band the energy contour passing through a given point with coordinates (q_xNa,q_yNa) has identical shape. The contour spacings vary from sub-band to sub-band, however. Thus knowledge of $E(q_x)$ for the two values $q_y=0$ and $q_y=\pi$ is sufficient to define the bands completely. In Fig. 4 a portion of the next sub-band is shown. The general features of this spectrum are in agreement with those of Brailsford[9] based on JWKB formulas.

Azbel[8] has shown that one can analyze the splitting of the magnetic sub-bands by writing the rational

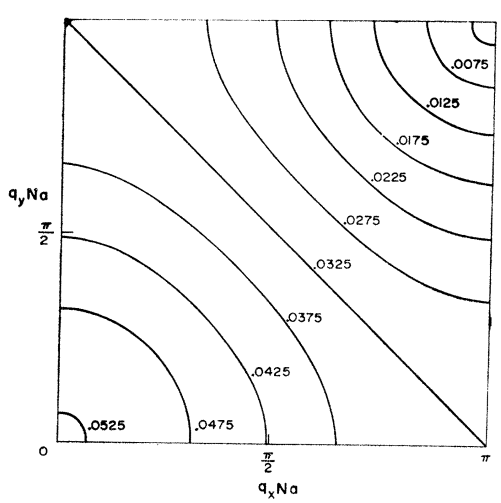

FIG. 3. Energy contours of magnetic sub-band near $E=0$, for $l/N=1/50$ (one-quarter of magnetic zone).

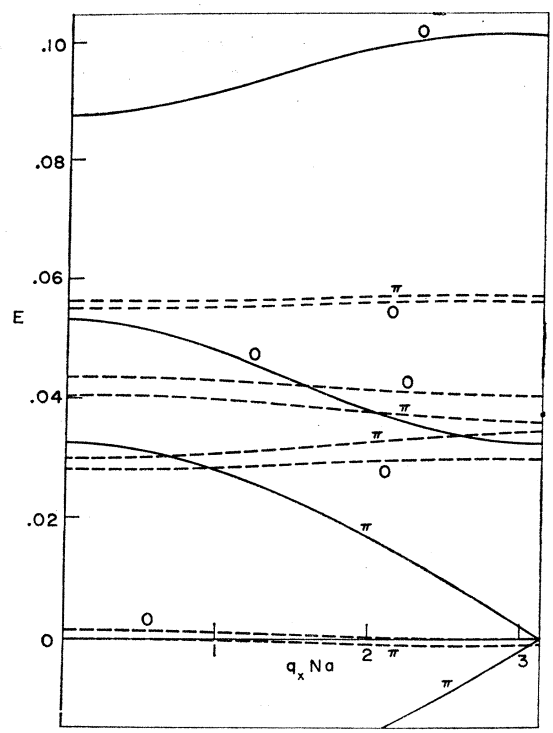

FIG. 4. Magnetic energy-band structure of broadened sub-bands near $E=0$. Solid curves correspond to $l/N=1/50$. Dashed curves correspond to $l/N=3/151$.

[9] A. D. Brailsford, Proc. Phys. Soc. (London) **A70**, 275 (1957).

number l/N as a continued fraction of the form

$$l/N=1/\{N_1+1/[N_2+1/(N_3+\cdots)]\}. \quad (12)$$

In this analysis one can regard the band splitting into N_1 sub-bands which in turn splits into N_2 sub-bands. This in turn splits into N_3, and so on. This is consistent with the result found here that when $l/N=3/151$, that each sub-band splits into three parts, with the exception that one extra sub-band appears. Azbel's formula gives only a semiquantitative description of the splitting since it predicts $N_1N_2N_3\cdots$ sub-bands, which is less than the exact number N. Nevertheless it was suggested by Chambers[6] that one might regard the split sub-bands as being derived from a parent sub-band by an analysis similar to the one for the sub-band in terms of the parent band. We therefore want to examine to what extent we can regard the spectrum for $l/N=3/151$ as being derived from the one for $l/N=1/50$. This corresponds to a 0.67% change in magnetic field, which is more than we would have liked to use. To get a smaller change, however, would have required using large values of N, which are not as convenient for calculations. We have investigated a few different cases for fields corresponding to values of l/N in the neighborhood of 1/50. The values of l/N considered are 1/49, 1/50, 1/51, 3/148, 3/151, 3/154, 19/956. The last of these can be written as $1/[50+1/(3+1/6)]$. The prediction for this one is that each of the sub-bands corresponding to $l/N=3/151$ breaks up into six smaller sub-bands. This is qualitatively correct although extra bands must appear since there have to be 956 sub-bands in all. In Fig. 5 we show how two of the broadened bands for $l/N=3/151$ split when $l/N=19/956$. In addition to the splitting of each band into six sub-bands, one extra band appears. This latter band may be regarded as arising from sub-band mixing. It should be noted that the sub-bands near the center of a cluster are broadened more than the others. This agrees qualitatively with what one might expect if an effective Hamiltonian based on $E(\mathbf{q})$ for $l/N=3/151$ is valid. However, a more quantitative test would have been possible if we split

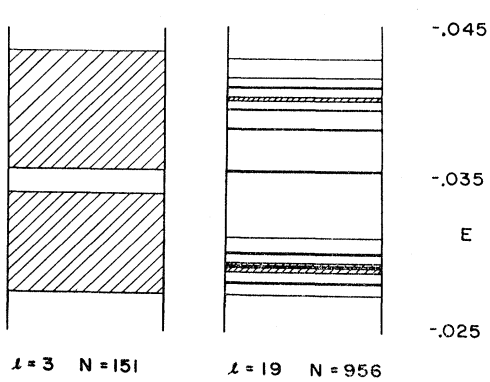

FIG. 5. Change in sub-band structure caused by small change in magnetic field.

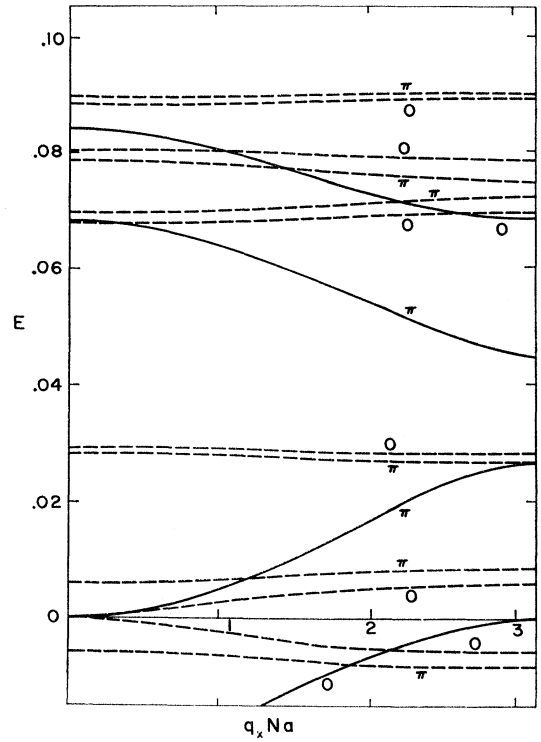

FIG. 6. Magnetic energy-band structure of broadened sub-bands near $E=0$. Solid curves correspond to $l/N=1/49$. Dashed curves correspond to $l/N=3/148$.

the sub-bands into a large number M of finer bands, where M is of the order of 20 or more. If an effective Hamiltonian based on a sub-band spectral function is valid, we would expect a number of discrete levels of the Onsager type. The discrete levels should correspond to orbits in $\mathbf{q}$ space given by $(n+\gamma)A_0$, where MA_0 is the area of the two-dimensional magnetic zone. The validity of this idea has to await more extensive calculations. The structure of the broadened bands for the remaining choices of l/N are shown in Figs. 4, 6, and 7.

Interband breakdown has been examined by means of a two-band model. We assume that the two bands result from the interaction of two simple overlapping bands. In our model the two energy-band functions $E^n(k_x,k_y)$ are the roots of the secular determinant

$$\begin{vmatrix} 2\cos k_x a-E & \Delta \\ \Delta & 2\cos k_y a-E \end{vmatrix}=0, \quad (13)$$

where Δ is an adjustable splitting parameter. The energy contours in each band are approximately squares with slightly rounded corners. In a repeated zone scheme these contours are arranged in a checkerboard pattern. An octant of a Brillouin zone is shown in Fig. 8. Magnetic-breakdown effects can be thought of as arising from tunneling between bands at the corners.

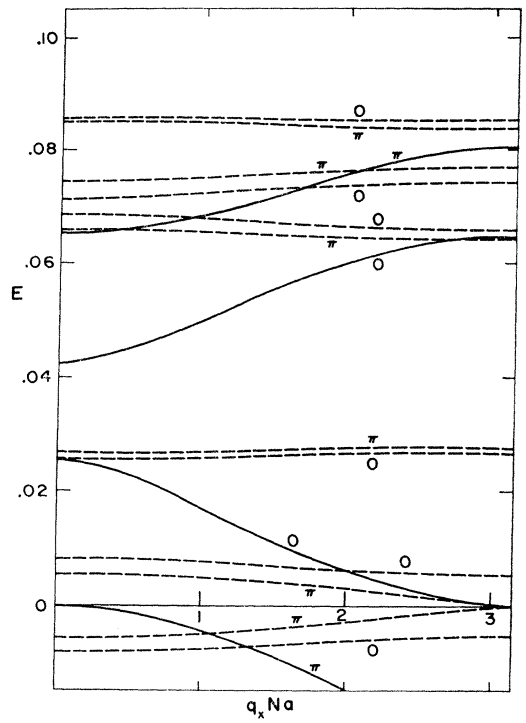

FIG. 7. Magnetic energy-band structure of broadened sub-bands near $E=0$. Solid curves correspond to $l/N=1/51$. Dashed curves correspond to $l/N=3/154$.

The two-band effective Hamiltonian leads to the coupled equations

$$u_{n-1}+u_{n+1}-Eu_n+\Delta v_n=0\,, \tag{14a}$$

$$\Delta u_n+[2\cos(n\phi+q_xa)-E]v_n=0\,, \tag{14b}$$

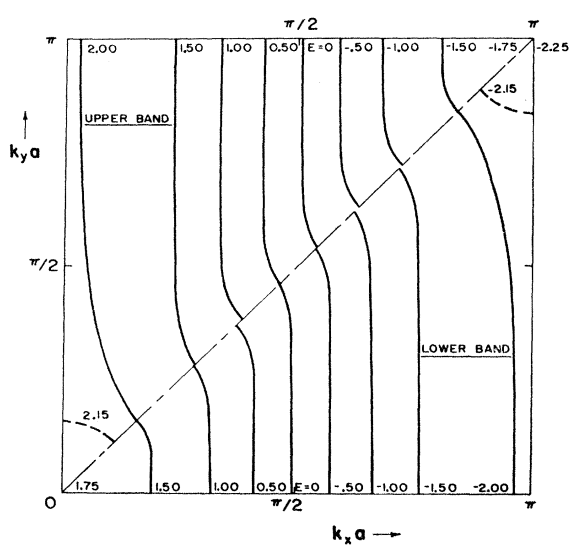

FIG. 8. Energy contours for two-band model $\Delta=0.25$. Each band has square symmetry about origin (one-quarter of Brillouin zone).

with the associated boundary conditions

$$u_{n+N}=e^{iq_yNa}u_n\,, \tag{15a}$$

$$v_{n+N}=e^{iq_yNa}v_n\,. \tag{15b}$$

This is transformed into a form suitable for calculation in the Appendix. The spectrum was obtained as a function of Δ, which is twice the band gap. Results for $l/N=1/50$ are shown in Fig. 9 for two portions of the spectrum where broadening occurs. In Fig. 9(b), broadening associated with interband breakdown is shown. For a large splitting parameter Δ, the levels are discrete and given to a good approximation by the Onsager prescription. Those associated with the lower band move down with Δ, while the levels in the upper band move up. A JWKB treatment of the interband

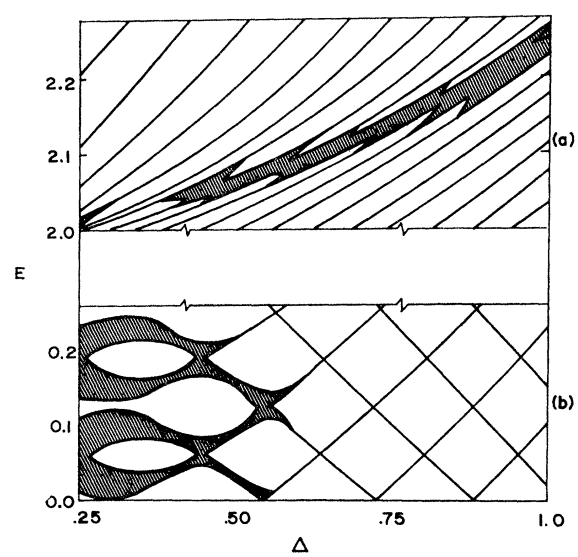

FIG. 9. Magnetic sub-band broadening for two-band model as a function of splitting parameter ($l/N=1/50$). (a) Portion of spectrum showing intraband breakdown. (b) Portion of spectrum showing interband breakdown.

tunneling problem yields a wave function which attenuates in tunneling between bands by a factor $\alpha=\exp\{-(\frac{5}{2}\Delta)^2\}$ in the neighborhood of $E=0$. (The JWKB results are consistent with the Blount tunneling criterion.) It should be noted that the sub-bands begin to broaden noticeably for $\Delta<0.6$ (corresponding to $\alpha=0.1$), and that the broadening is largest when a type of resonance associated with crossing discrete levels occurs. The broadening shown in Fig. 9(a) is associated with intraband tunneling.

III. CONCLUSIONS

The model calculations carried out in this paper illustrate the complexities of the magnetic spectrum in simple geometries for simple bands. The parameter l/N

which we have considered corresponds to fields much greater than presently available. Nevertheless the first-order correction given by Roth to the Onsager area quantization yields almost perfect agreement with our calculations. The fine structure in the broadened regions, associated with breakdown, is in qualitative agreement with Azbel's description. Similar results are expected for more general bands. It is not likely that such structure will be observed experimentally until much larger magnetic fields are available. The results depend on long-range order, and crystal imperfections as well as electron-phonon interactions tend to obscure such fine structure. Uniformity of the magnetic field is also crucial unless one is dealing with extremely large fields.

ACKNOWLEDGMENTS

The authors would like to thank Dr. F. K. Bloom, Dr. D. Gray, and P. Kapo for helpful discussions. They would especially like to thank Dr. W. G. Chambers for suggesting some of the problems and methods of analysis.

APPENDIX

In this section the matrix equations for the one- and two-band models are put in a form suitable for obtaining the magnetic band structure. We consider the simple square lattice in which the only nonzero Fourier coefficients of $E(\mathbf{k})$ are $\epsilon(\pm 1, 0)=\epsilon(0, \pm 1)=\epsilon_1$, and $\epsilon(\pm 1, \pm 1)=\epsilon(\mp 1, \pm 1)=\epsilon_2$. In terms of these parameters Eq. (7) becomes

$$\mathbf{U}_{n-1}=\mathbf{T}_n(q_x)\mathbf{U}_n\,, \tag{A1}$$

where $\mathbf{U}_n$ is the two-component column vector with elements (u_n, u_{n+1}) and $\mathbf{T}_n(q_x)$ is the square matrix with elements

$$\begin{aligned}
T_{11}&=[E-2\epsilon_1\cos(q_xa+n\phi)]\\
&\qquad\times\{\epsilon_1+2\epsilon_2\cos[q_xa+(n-\tfrac{1}{2})\phi]\}^{-1},\\
T_{12}&=-\{\epsilon_1+2\epsilon_2\cos[q_xa+(n+\tfrac{1}{2})\phi]\}\\
&\qquad\times\{\epsilon_1+2\epsilon_2\cos[q_xa+(n-\tfrac{1}{2})\phi]\}^{-1},\\
T_{21}&=1\,,\\
T_{22}&=0\,.
\end{aligned} \tag{A2}$$

We now define

$$\mathbf{T}(q_x)=\prod_{n=1}^{N}\mathbf{T}_n(q_x)\,. \tag{A3}$$

From Eqs. A1 and A3, and making use of the boundary conditions on $\mathbf{U}$, it follows that

$$\mathbf{U}_1=\mathbf{T}(q_x)\mathbf{U}_N=e^{-iNq_ya}\mathbf{U}_N\,. \tag{A4}$$

This leads to the secular equation

$$\det[\mathbf{T}(q_x)-e^{-iNq_ya}\mathbf{1}]=0\,, \tag{A5}$$

where $\mathbf{1}$ is the unit matrix. This yields

$$e^{-i2Nq_ya}-e^{-iNq_ya}\,\mathrm{Tr}[\mathbf{T}(q_x)]+\det[\mathbf{T}(q_x)]=0\,. \tag{A6}$$

The determinant can be evaluated by multiplying the determinants of the matrices $\mathbf{T}_n(q_x)$. It is a simple calculation and the result is $\det\mathbf{T}(q_x)=1$. From Eq. (A6) one then obtains

$$\mathrm{Tr}[\mathbf{T}(q_x)]=2\cos Nq_ya\,. \tag{A7}$$

In order to evaluate the trace of $\mathbf{T}(q_x)$ we first write each factor $\mathbf{T}_n(q_x)$ in the form

$$\mathbf{T}_n(q_x)=\{\epsilon_1+2\epsilon_2\cos[q_xa+(n-\tfrac{1}{2})\phi]\}^{-1}\mathbf{A}_n(q_x)\,. \tag{A8}$$

The matrix $\mathbf{T}(q_x)$ can then be expressed in terms of the products of the matrices $\mathbf{A}_n(q_x)$ and a factor Q^{-1}, where Q is given by

$$Q=(2\epsilon_2)^N\prod_{n=1}^{N}x_n\,, \tag{A9}$$

where $x_n=\epsilon_1/2\epsilon_2+\cos(n\phi+\delta)$ and $\delta=q_xa-\frac{1}{2}\phi$. We will now show that the factors x_n are the N roots of a polynomial of degree N. We introduce the Tschebychev polynomials $f_m(z)$ defined by the relations

$$\begin{aligned}
f_0(z)&\equiv 1\,,\\
f_1(z)&\equiv z\,,\\
&\vdots\\
f_{m+1}(z)&=2zf_m(z)-f_{m-1}(z)\,.
\end{aligned} \tag{A10}$$

It is a matter of simple induction to see that

$$f_m(\cos\theta)\equiv\cos m\theta\,. \tag{A11}$$

We see from the definition of x_n that

$$\begin{aligned}
f_N(x_n-\epsilon_1/2\epsilon_2)&=f_N[\cos(n\phi+\delta)]\\
&=\cos N\delta\,,
\end{aligned} \tag{A12}$$

where we have made use of the fact that $nN\phi$ is a multiple of 2π. The x_n are thus roots of the polynomial

$$P_N(x)\equiv f_N(x-\epsilon_1/2\epsilon_2)-\cos N\delta\,. \tag{A13}$$

Thus

$$P_N(x)\equiv\sum_{n=0}^{N}a_nx^n=a_N\prod_{n=1}^{N}(x-x_n)\,. \tag{A14}$$

We note from Eq. (A10), for $N\geqslant 1$, that $a_N=2^{N-1}$. It thus follows simply that

$$\begin{aligned}
\prod_{n=1}^{N}x_n&=2(-\tfrac{1}{2})^NP_N(0)\\
&=2(-\tfrac{1}{2})^N[f_N(-\epsilon_1/2\epsilon_2)-\cos N\delta]\,.
\end{aligned} \tag{A15}$$

We define α by the relation $\cos\alpha=-\epsilon_1/2\epsilon_2$ and make use of Eqs. (A9), (A11), and (A15). We obtain

$$Q=2(-\epsilon_2)^N[\cos N\alpha-\cos N\delta]\,. \tag{A16}$$

We now have to evaluate the trace of the matrix $\mathbf{A}(q_x)$, where

$$\mathbf{A}(q_x)=\prod\mathbf{A}_n(q_x).$$

We note that $A_n(q_x+2\pi/Na)=A_{n-M}(q_x)$, where $Ml=1$, mod N. Thus replacing q_x by $q_x+2\pi/Na$ corresponds to a cyclic permutation of the matrices $\mathbf{A}_n(q_x)$ and does not affect the trace of $\mathbf{A}(q_x)$. The trace is thus periodic in q_x, with periodicity $2\pi/Na$. It follows that

$$\mathrm{Tr}[\mathbf{A}(q_x)]=C_0+C_1e^{iNaq_x}+C_1^*e^{-iNaq_x}. \quad \text{(A17)}$$

There are no higher powers in the Fourier series since the highest contribution from the individual matrices $\mathbf{A}_n(q_x)$ is e^{iaq_x}, and there are just N matrices. The coefficient C_1 is obtained by dropping all terms in $\mathbf{A}_n(q_x)$ except those which are proportional to e^{iaq_x}. It is convenient to factor, out of what remains, the term $\epsilon_2e^{in\phi}$ and express the ratio ϵ_1/ϵ_2 in terms of α, as before. This leads directly to the result

$$C_1=\epsilon_2{}^N\prod_{n=1}^{N}e^{in\phi}\,\mathrm{Tr}[\mathbf{M}^N], \quad \text{(A18)}$$

where $M_{11}=2\cos\alpha$, $M_{12}=-M_{21}=-e^{i\phi/2}$, $M_{22}=0$, and $\phi=2\pi l/N$. The product over n leads to a factor $(-1)^{l(N-1)}$. This can be simplified to $(-1)^{N-1}$ since if $(N-1)$ is odd l must also be odd, or else l and N would have 2 as a common factor, and not be in lowest terms. The trace is obtained by diagonalizing $\mathbf{M}$ first. The end result is simply

$$C_1=2(-1)^{N-1}\epsilon_2{}^N\cos N\alpha. \quad \text{(A19)}$$

It is a simple matter to find C_0 from Eq. (A17) in terms of $\mathrm{Tr}[\mathbf{A}(0)]$ or finally in terms of $\mathrm{Tr}[\mathbf{T}(0)]$. Combining these results it is found that

$$f(q_x,q_y)=\tfrac{1}{2}[\cos N\alpha+(-1)^{l+1}]\,\mathrm{Tr}[\mathbf{T}(0)], \quad \text{(A20)}$$

where

$$f(q_x,q_y)\equiv\cos N\alpha[\cos Naq_y+\cos Naq_x-1]-(-1)^l\cos Naq_x\cos Naq_y, \quad \text{(A21)}$$

and $\cos\alpha=-\epsilon_1/\epsilon_2$. Equation (A20) is the desired result. The trace of the matrix $\mathbf{T}(0)$ is evaluated for various values of the energy E by means of an electronic computer. Only for certain ranges of E can Eq. (A20) be satisfied for real q_x, q_y. It follows from Eq. (A20) that the shapes of the energy contours are identical for all sub-bands. In the case considered here $\epsilon_2=0$ and Eq. (A20) becomes

$$\cos Naq_x+\cos Naq_y=1+\tfrac{1}{2}\,\mathrm{Tr}[\mathbf{T}(0)]. \quad \text{(A22)}$$

The two-band model can be handled in a similar way. We solve Eq. (14b) for v_n in terms of u_n and substitute into Eq. (14a), thereby arriving at the result

$$\mathbf{U}_{n-1}=\mathbf{F}_n(q_x)\mathbf{U}_n, \quad \text{(A23)}$$

where $\mathbf{F}$ is the matrix with coefficients

$$F_{11}=E+\Delta^2[2\cos(n\phi+q_xa)-E]^{-1},$$
$$F_{12}=-F_{21}=-1,\quad F_{22}=0. \quad \text{(A24)}$$

We define λ such that $2\cos\lambda\equiv E$ and let

$$\mathbf{A}_n(q_x)=2[\cos(n\phi+q_xa)-\cos\lambda]\mathbf{F}_n(q_x). \quad \text{(A25)}$$

The procedure from this point is quite similar to the previous one. The result is

$$g(q_x,q_y)=\tfrac{1}{2}(1-\cos N\lambda)\,\mathrm{Tr}[\mathbf{F}(0)]-\cos N\lambda, \quad \text{(A26)}$$

where

$$g(q_x,q_y)\equiv\cos(Naq_x)\cos(Naq_y)-\cos N\lambda(\cos Naq_x+\cos Naq_y) \quad \text{(A27)}$$

and

$$\mathbf{F}(q_x)=\prod_{n=1}^{N}\mathbf{F}_n(q_x).$$

It should be noted that $g(q_x,q_y)$ depends on E so that in this case the energy contours in $\mathbf{q}$ space will generally have different shapes in different bands.